IMAGE PROCESSING FOR HYDRAULIC JUMP FREE-SURFACE DETECTION

ROBERT LJUBIČIĆ(1), IVANA VIĆANOVIĆ(2), BUDO ZINDOVIĆ(3), RADOMIR KAPOR(4) & LJUBODRAG SAVIĆ(5)

(1,2,3,4,5) Civil Engineering Faculty, University of Belgrade, Serbia
e-mail: rljubicic@grf.bg.ac.rs; vicanovicka@gmail.com; bzindovic@grf.bg.ac.rs; rkapor@grf.bg.ac.rs; ljdsavic@grf.bg.ac.rs

ABSTRACT

Hydraulic jumps exhibit a high degree of free-surface oscillations, triggered by intense turbulence and aeration. These processes are difficult to model numerically and are frequently investigated on a scale model. However, measuring the oscillatory characteristics of the hydraulic jump is not without issues, as the majority of available methods are not intended for tracking instantaneous depth profile or free-surface interface (FSI). Some methods are limited to a selected set of few predetermined points, and are sensitive to variations of secondary characteristics of the hydraulic jump: point gauges are sensitive to aeration rate and rate of the free-surface changes, electroconductive and optical probes require direct contact with the air-water mixture (disrupting the free surface), while the ultrasonic distance measurement accuracy is severely impacted by the shape of the free surface and aeration rate. To alleviate these issues, we propose the application of the non-intrusive method based on image processing techniques to detect the instantaneous FSI. The first step is to record the free-surface region in a series of images, with a predefined constant time shift. Subsequently, the FSI along the hydraulic jump is detected in every image. Presented method was used to reconstruct temporal evolution of the depth profile from the FSI position in the recorded images. The obtained dominant FSI oscillation frequencies along the hydraulic jump show good agreement with previous research. Results also show that the proposed approach is more robust than previously available methods – minor sensitivity to camera shooting angle, rate of the free-surface change, surface aeration variability, etc. Method is also very simple, with only a few tunable parameters, and affordable, as the only required equipment is a camera. The preprocessing and calibration steps needed to obtain reliable data for further processing are also described. Using method presented in this paper, one can gain a better understanding of the characteristics of the hydraulic jump: instantaneous and time-averaged FSI profile, as well as the frequency spectrum of FSI variations along the hydraulic jump. This can be useful for the design of hydraulic structures, in particular – the hydraulic jump stilling basins.

Keywords: image processing; hydraulic jump; depth measurement; hydraulic model

1 INTRODUCTION

Reliable information on depths and their temporal evolution is crucial for any hydraulic analysis, as it provides basic information about the water flow. Water depth detection and tracking, a seemingly simple hydraulic research task, has proven to be rather challenging. For flow in the hydraulic jump, depth measurement presents an even greater challenge due to high frequency oscillations and intense surface aeration. These unfavorable conditions can be present in both field and laboratory settings.

Traditional depth measuring equipment can display intrinsic unreliability and measurement uncertainty. Point gauges are unable to track free-surface oscillations. Ultrasonic (US) sensors are sensitive to free-surface aeration, surface angle relative to the sensor, and the ejection of droplets from the air-water mixture (Bung, 2013; Kucukali & Chanson, 2008; Murzyn & Chanson, 2009). LIDAR scanning can provide a detailed spatial description of the free-surface, but the required equipment is expensive and difficult to operate (Montano, Li, & Felder, 2018). Depth measurement using electroconductivity probes is intrusive, can be time-consuming, and can only provide an average depth estimate. Over the course of the last two decades, techniques based on image-processing have become a popular alternative to traditional methods for monitoring hydraulic parameters such as depth, surface velocity, air-concentrations, etc. The appeal of image-based methods lies within their non-intrusive approach, relatively simple setup procedure, and low equipment cost. In general, several different image-based applications have been considered by researchers: (1) depth measurement/free-surface detection and tracking, (2) velocity measurements, (3) air-concentration estimation, etc.

For free-surface interface (FSI) detection and tracking from a camera recordings, several approaches are predominantly used: (1) global thresholding based on contrast, brightness and/or color, (2) adaptive (local) thresholding, (3) edge detection, (4) temporal analysis of frame sequences, (5) machine learning-based detection. Global thresholding methods, while usually simpler, require higher control over environmental variables such as lighting, and in some cases can involve tracers or dyes in order to accentuate water in captured images. Adaptive thresholding and edge detection-based methods are more robust in terms of

environmental factors but can often provide false detections in an image (outliers) that can be difficult to filter. Temporal analysis can be used to detect the water level based on differences in sequential images but requires distinct features with sharp interfaces in every image. Machine learning techniques are relatively new but developed at a fairly fast pace, and, while they offer possibility to address the issues of previous methods, their applicability for hydraulic measurements is still to be investigated.

One of the first attempts at image-based investigation of the open channel flow was presented by Mossa and Tolve (1998) for aerated hydraulic jumps in laboratory conditions. They successfully applied image processing to investigate the distribution of air-concentration in the entire hydraulic jump region. Leandro et al. (2012) furthered the idea about the estimation of the amount of entrained air in air-water mixtures from pixel densities in acquired images. While innovative and non-intrusive, the authors concluded that the biggest issue of the method is the need for calibration and that results are representative only in the vicinity of the flume wall. Lennon and Hill (2006) used a simple thresholding method for FSI level detection and Particle Image Velocimetry (PIV) to study the streamwise velocity distribution in an undular hydraulic jump. They used a laser light sheet to illuminate the centerline of the flume and accentuate the tracer particles. Bung (2013) used a high-speed camera at 1220 frames per second (fps) in order to investigate the free-surface roughness in strongly aerated chute flow by using image contrast enhancement and subsequent edge detection. He attempted to verify his results using an US sensor. However, because of the penetration of the acoustic signal in the air-water mixture, large discrepancy was found from EC-based measurements. Nevertheless, he managed to conclude that surface roughness increases for stepped chutes, when compared to the smooth chutes. Nóbrega, Schulz and Zhu (2014) attempted an approach with a high-speed camera and a laser light sheet setup, while the free surface interface was detected by global thresholding on a grayscale image. However, they wrongly presumed that the US sensor, used for verification, would provide accurate estimate for depths in a hydraulic jump, as proven by previous research (Bung, 2013; Kucukali & Chanson, 2008; Murzyn & Chanson, 2009).

Misra et al. (2006) used a more advanced free surface detection method based on texture segmentation by gray level co-occurrence matrices and additional post processing using active contours minimizing energy functionals. They have also used a laser light sheet to illuminate the target area. Yu and Hahn (2010) developed an image-based method for water level monitoring based on the gradient detection using Sobel-Feldman operator, but their experiment had a noticeably small area covered by ground control points that are used for image transformations, and they were positioned far from the region of interest (ROI). Parasuraman et al. (2012) applied their image-based water level detection algorithm to provide real-time monitoring in a small channel in Singapore. The algorithm was based on edge detection in a high contrast target area on the channel wall, with a subsequent application of Hough transformation to detect the straight line which represents the water level. Their results were successfully verified by radar measurements. A similar approach (Hasan et al., 2016) was later implemented for an in-situ flood warning system, improved by using an infrared projector and dedicated day and night cameras. Viriyakijja and Chinnarasri (2015) used Canny edge detection for laboratory flume wave depth measurements. Although the method was applied to a relatively small target area, they concluded that recordings from a camera could potentially replace wave gauge measurements with adequate accuracy, with an important quality of non-intrusiveness. While most depth/level detection methods used a fixed camera setup and assumed that no camera movement or vibrations were present during the recording period, Lin, Lin and Han (2018) developed a more robust approach that could alleviate for camera movement through least-square matching and normalized cross-correlation procedures.

Our paper presents a simple method for hydraulic jump FSI detection and tracking, based on the analysis of image gradients. Results of this method were compared to the results obtained with contrast-based method used in a majority of previous research. Gradient analysis, as opposed to simple thresholding techniques, can easily be tuned to capture the boundary between the water and the background, even in the presence of strong image noise, spatial and temporal changes in surface aeration, lighting conditions, etc. This, in turn, significantly improves the quality of the FSI detection. Described approach can allow for easier and better spatio-temporal analysis of hydraulic jumps – estimation of depth distribution: maximum, minimum and average depths along the jump profile, frequency analysis using Fast Fourier Transform (FFT) to obtain the spectral properties of the hydraulic jump.

Along with the FSI detection methodology, special attention was paid to the analysis of the impact of data preprocessing, experiment preparation, and postprocessing procedures, in order to improve the accuracy of both methods.

In Section 2, both methods for FSI detection are described: first the contrast-based, and then a gradient method. In Section 3, presented methods have been applied to the camera recordings of hydraulic jumps in a laboratory flume for two cases: (a) high surface aeration, and (b) moderate to low surface aeration. Results from both methods were compared and discussed. It was demonstrated that the gradient-based method outperforms the simpler contrast-based thresholding approach, especially in conditions of low and/or varying surface aeration, where the latter method fails completely. With the proposed image-based approach, one can obtain a greater insight into the behavior of hydraulic jumps than with traditional measurement methods.

2 MATERIALS AND METHODS

In this section, algorithms of two image-based methods for FSI detection in hydraulic jumps are presented: contrast- and gradient-based. The outline of both presented algorithms can be summarized into four steps:

(a) Data preparation: splitting the video into frames and elimination of distortion (rectification) caused by the imperfections of the specific camera,
(b) Detection of Control Points, mapping of real-world to pixel-space coordinates, and orthorectification of images using CPs,
(c) Filtering to reduce noise and accentuate the specific features in images, color-space transformation, and parameter calibration to improve the detection accuracy,
(d) Detection of the free-surface interface with optional postprocessing to reduce the false positives.

Steps (a) and (b) are method-invariant and are described in Section 2.1. Steps (c) and (d) are dependent on the choice of the FSI detection method and, as such, are described separately for contrast-based and gradient-based approaches.

2.1 Calibration and preprocessing

In order to obtain adequate results from the image data, intrinsic (internal), extrinsic (position and orientation) and lens distortion camera parameters must be determined prior to image processing. Intrinsic parameters include focal length, principal point, skewness coefficient. Additionally, radial and tangential distortion of the camera lens have to be determined as they have a significant impact on quality of the results. Extrinsic parameters, that relate the real-world 3D points (Control Points) with previously determined locations to their pixel coordinates, depend on the actual experimental setup and can be a major source of errors (MathWorks, 2019b).

With respect to the position of the camera relative to the surface, two approaches can be used:

(a) Recording of the wall surface closer to the camera, and
(b) Recording of the opposing wall surface.

While the first approach is somewhat easier to set up, three things need to be considered. First, the thickness of the flume wall can cause light refraction in the flume wall and distort the detected FSI inside the flume, while the amount of refraction-induced error depends on the wall material and its thickness. Also, the distance between the CPs and the actual ROI plane is a source of errors on its own. Second, since the aeration in the jump varies with depth, additional noise can appear in the image which requires filtering. Third, the camera must always be positioned in such a way that it records only the FSI on the flume wall closest to the camera to avoid false detections from the image background.

In the experiments described in this paper, CP markers were positioned on the acrylic wall surface of the flume. In order to allow an easy detection of the CPs, they were chosen to be of different color from the other features in the image. If possible, all CPs should be positioned in such a way that they always remain outside of the ROI. This way, the transformation of real-world to pixel coordinates for the ROI relies solely on the interpolation between CPs and not on the extrapolation outside the CP-covered area. This can ensure better accuracy of the orthorectification procedure because the distortion between CPs can be assumed linear, while this cannot be guaranteed for the region outside this area. Although the minimal number of required CPs for homographic coordinate system transformation is four, due to tangential field distortion, using at least 6-8 CPs is recommended.

Detection of CPs can be done in two ways: (1) manually, based on a sample image, or (2) automatically for every frame. Manual selection of CPs is fairly straightforward but assumes that the camera position and orientation remain unchanged during the experiment, and that the effect of vibrations is neglectable for both the camera and the ROI. This is safe to assume for shorter experiments, but the relative camera position can change during long recordings in such a way that it produces biased results.

Captured images usually contain sharp local variations in pixel intensity and color, i.e. “salt-and-pepper” noise. To reduce this noise, i.e. increase the signal-to-noise ratio in the image, median blur filter can be used, which takes the median of all pixels in the defined kernel area (pixel neighborhood) and replaces the central pixel with the kernel’s median. Unlike Gaussian blur, median filter is an edge-preserving method which generally retains sharp features in the image, such as the FSI. In cases of significant noise, additional edge-preserving bilateral filtering method is recommended (Tomasi & Manduchi, 1998).

2.2 Contrast-based FSI detection

In this chapter, a simple contrast-based method for detecting water surface in a hydraulic jump is presented. As shown in Section 3, this method is best suited for hydraulic jumps with high surface aeration. The presented method is similar to the one presented by Nóbrega, Schulz and Zhu (2014), but more robust in the presence of noise due to the advanced calibration, pre- and postprocessing procedures. The outline of the method is presented in Figure 1.

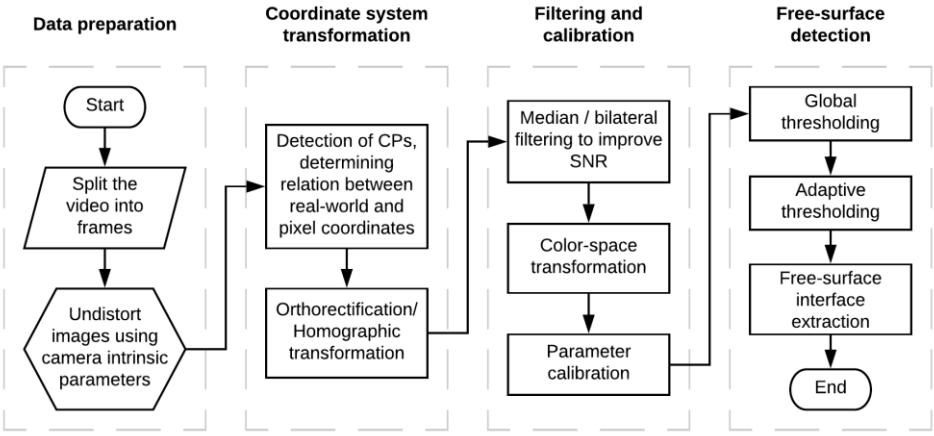

Figure 1. Outline of the contrast-based FSI detection procedure

Once the image has been orthorectified using CPs and the ROI has been selected, image color-space can be converted from RGB (red, green, blue) to grayscale color-space using the transformation function (IEC, 1999):

$$Y(x,y) = 0.2126R(x,y) + 0.7152G(x,y) + 0.0722B(x,y) \quad [1]$$

where $Y(x, y)$ is the grayscale value for the pixel at the (x, y) position in the image, while R, G, and B are red, blue and green channel values for pixel (x, y) in the original image, represented in floating point [0,1] range.

Global thresholding on a grayscale color-space separates regions in the image based on their pixel value $Y(x, y)$. This produces a so-called binary image (pixels can have only two values, Figure 2-left):

$$Y_{G\_th}(x,y) = \begin{cases} 1 & ,Y(x,y) > Th \\ 0 & ,otherwise \end{cases}, \quad [2]$$

where Th is the threshold value. Threshold value should be chosen so that the boundary between regions where $Y_{G\_th} = 1$ and $Y_{G\_th} = 0$ represents the FSI. Determining the threshold parameter that can adequately separate the water surface from the flume wall is crucial for the algorithm. Although this can be performed manually based on a sample image, a more adaptive approach is recommended. One such approach is to manually determine the threshold parameter for a small subset of images (i.e. keyframes, every Nth frame), and then apply a search across a range of threshold parameters to determine the value which best fits the keyframe data. Criteria for estimating the impact of selected threshold parameters on the quality of reconstruction of the FSI is the root mean square difference (RMSD) between manually and automatically detected FSI levels.

Figure 2. Left – Binarized image using global thresholding; Right – Original image with the FSI from contrast thresholding.

In order to detect the edges in the binary image, an adaptive thresholding procedure is performed. The adaptive threshold approach uses the same core method as the global threshold function, with the only difference being that the algorithm obtains the threshold value as the mean of a kernel, $T(x,y)$, around each pixel (Figure 2-right):

$$Y_{A\_th}(x,y) = \begin{cases} 1 & ,Y_{G\_th}(x,y) > T(x,y) \\ 0 & ,otherwise \end{cases}. \quad [3]$$

2.3 Gradient-based FSI detection

The main shortcoming of the previous method is the parameter calibration process and parameter sensitivity. High parameter sensitivity in conditions with significant contrast variability and noise makes the performance of the contrast-based method inherently case-specific (as shown in Figures 5 and 8). In order to alleviate those issues and provide a more robust approach, a gradient analysis-based method is proposed in this research. This approach aims to identify the boundary between the water surface and the flume wall based on the local variability of the color intensity. Additionally, since the direction of the FSI in the image is predominantly horizontal, accuracy of the method is improved significantly when vertical gradients are considered only.

Vertical gradient of any pixel neighborhood can be determined using the Sobel-Feldman operator (Sobel, 2015) which convolves a specific square kernel of size n, K_{yn}, with any single-channel representation of the original image:

$$G_{yn} = K_{yn} * Y, \quad [4]$$

where Y is a single-channel representation of the original image (e.g. grayscale, red, blue, green, etc.). Although the Sobel-Feldman operator originally uses a 3x3 kernel, the same principles can be used to obtain an arbitrary-sized kernel (Sobel, 2015). The result of this discrete linear convolution presents an approximation of the first derivative of the image pixel intensity in vertical direction – the vertical gradient map (Figure 3).

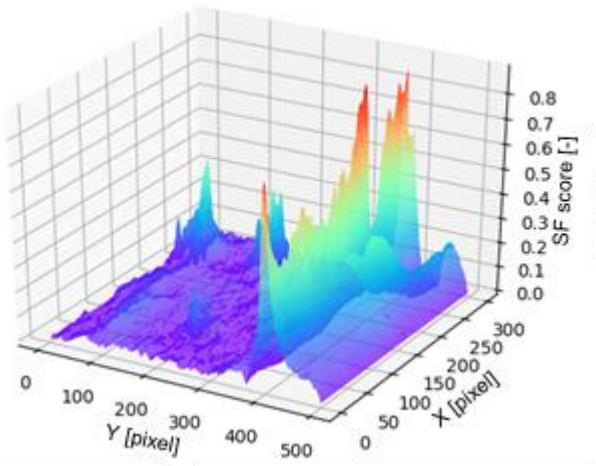

Figure 3. Example of a vertical gradient map obtained using Sobel-Feldman operator; Ridge spanning in the X direction indicates a probable FSI.

Selection of the appropriate image channel for gradient mapping is very important as some channels can have higher signal-to-noise ratio (SNR). Optimal choice should be based on the visual analysis of the colors available in the image or can be determined on a sample image. Instead of G_{yn}, the absolute value of the gradient map, $|G_{yn}|$, is often preferred, which treats both directions of the intensity change equally (high→low, low→high). From the $|G_{yn}|$, the approximation of the FSI can be obtained by searching for the maximal value in each column, C, of the gradient map:

$$W(x) = \underset{C \subset |G_{yn}|}{\arg\max}\left(C(x)\right), \quad [5]$$

where $W(x)$ is the vector that contains the pixel-space coordinates of the FSI, $C(x)$ is the image column at position x, containing pixel gradients in vertical direction. Additional filtering can be performed at this point, to reduce the number of false positive detections. While many rough errors can be detected by using distance or gradient limiting filters (to eliminate large discontinuities in the $W(x)$), additional SNR improvements based on median filter and/or Savitzky-Golay filter are highly recommended for data smoothing. The outline of the gradient-based method is presented in Figure 4. From the position of the CPs (both real-world and in-image), the relationship between the pixel-space and the real-world coordinates can easily be determined, which can then be used to transform the $W(x)$ into the depth profile along the hydraulic jump.

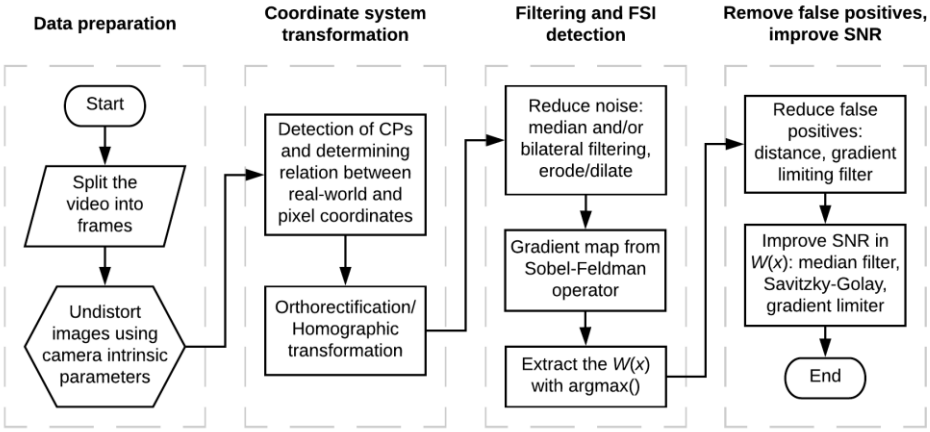

Figure 4. Outline of the proposed gradient-based FSI detection procedure

2.4 Experimental setup

In order to examine the viability of the proposed methods, an experimental setup was created in the Hydraulic laboratory of the Civil Engineering Faculty at the University of Belgrade. The setup consisted of a scale model of a stepped spillway with a stilling basin, both 0.46 m in width. Discharge was measured using a twin V-notch weir and verified with an ultrasonic flow meter. Downstream depth was controlled using a sluice gate. More detailed description of the laboratory flume is presented in Ljubicic et al. (2018). Video was obtained using a tripod-mounted Sony RX10II camera at 4K resolution (3840 by 2160 pixels) at 29.97 frames per second. Camera intrinsic and lens distortion parameters were determined using MATLAB® Camera Calibrator App (MathWorks, 2019a).

3 RESULTS AND DISCUSSION

In this section, results from two experiments with different flow conditions are presented:

(a) High free-surface aeration, at 38.3 L/s (inflow Froude number of 8.3),

(b) Moderate to low free-surface aeration, at 20.7 L/s (inflow Froude number of 9.4).

In both experiments, A-type hydraulic jump was established. Due to restrictions in laboratory space, only opposing wall recording was performed. Both experiments used a black backboard for contrast enhancement. In total, 16 CPs mounted on the opposing wall were used for both experiments (green markers in Figures 5 and 8). Three additional check points were used to assess the quality of the orthorectification (yellow markers). Orthorectification was performed using CPs that were visible in every frame during each experiment. For each of the experiments, a single video of approximately 30 seconds was recorded and processed. For both methods, grayscale map was used as a single-channel representation of the original image. Same preprocessing filters and filter parameters were used by each of the methods, to provide a fair comparison of performance.

For highly aerated jumps, both contrast- and gradient-based methods provided good agreement with the experimental observation across the entire ROI. Results for three sample frames are presented in Figure 5, for both methods. While the superiority of the gradient approach over contrast approach diminishes in high surface aeration conditions with low aeration variability along the jump, the former is significantly easier to calibrate, and produces fewer false positives (Figure 5). It is important to note that the contrast-based approach yields somewhat higher average depths in the central region of the hydraulic jump, with an average difference of 4 mm.

Statistics for the depth profile in the ROI (Figure 6) show that the time averaged depth increases approx. 2.5 times in the downstream direction, while the standard deviation of depth oscillations decreases by approx. 20%. Results also show that the envelopes of maximal and minimal depth for both methods are in good agreement. Fast Fourier Transform (FFT) spectrums for results from both methods show a strong agreement, and the dominant frequency of depth oscillations in the ROI is approx. 2.1 Hz (Figure 7). This value is in agreement with findings of Montano, Li, and Felder (2018) for hydraulic jumps with similar inflow Froude number.

By reducing the discharge, regions with lower free-surface aeration begin to appear, initially in the downstream part of the hydraulic jump. This hinders the ability of the contrast-based method to adequately capture the FSI in those regions (Figure 8). Additional difficulty is the slight change in scene lighting in the righthand side of the image. To alleviate these issues, one approach can be to separate the regions in the image, based on the surface aeration intensity and apply different parameters to each region, as in Nóbrega, Schulz and Zhu (2014). However, this conflicts with the main intention of the image-processing approach – to provide a simple and robust mean of instantaneous depth tracking. The gradient method was able to capture the features of the free-surface with very little false detections, regardless of the surface aeration variability. Identical set of parameters were used for the gradient method in both experiments, which provided an additional validation of its simplicity and robustness.

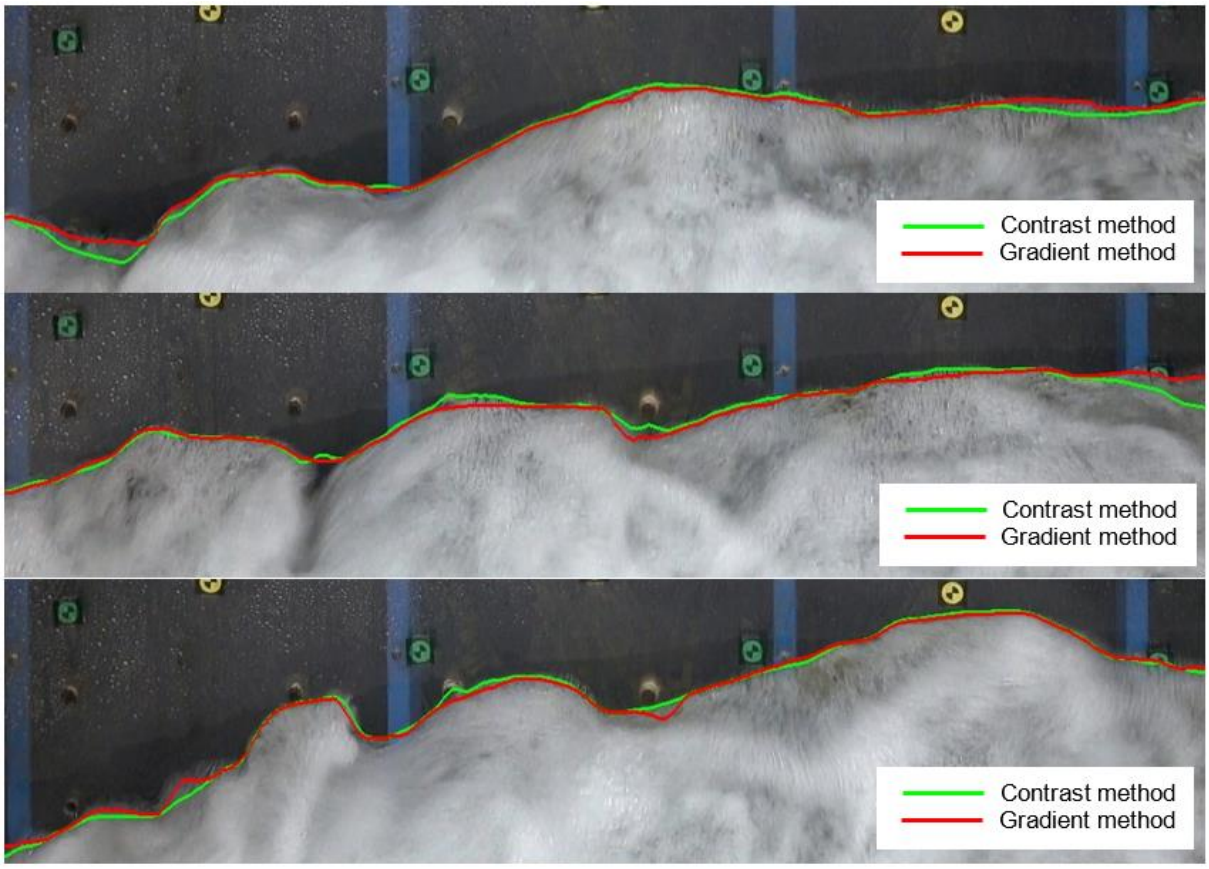

Figure 5. FSI detection for high surface aeration conditions at 38.3 L/s at different time instances.

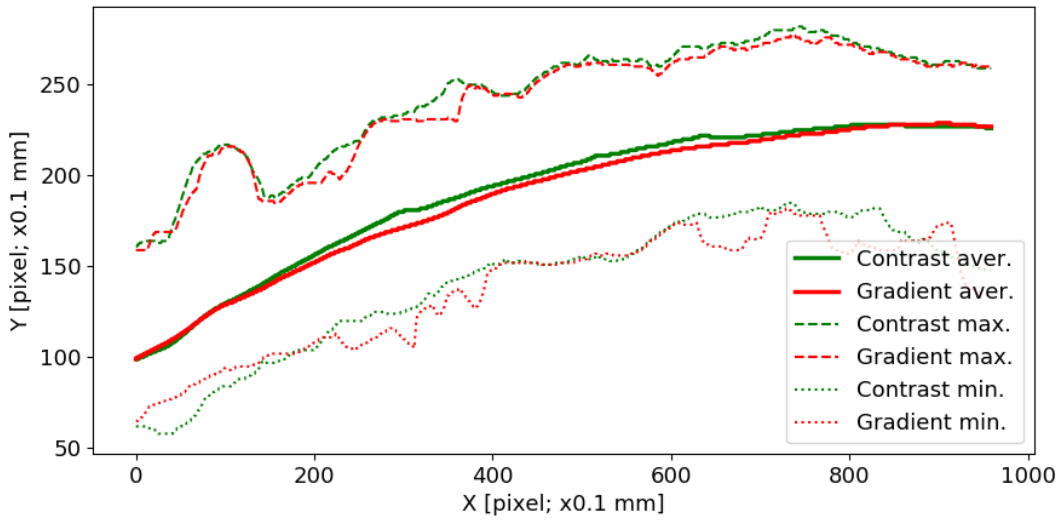

Figure 6. Statistics of the FSI profile along the hydraulic jump for both methods in high surface aeration conditions: averages, maximums, minimums along the hydraulic jump.

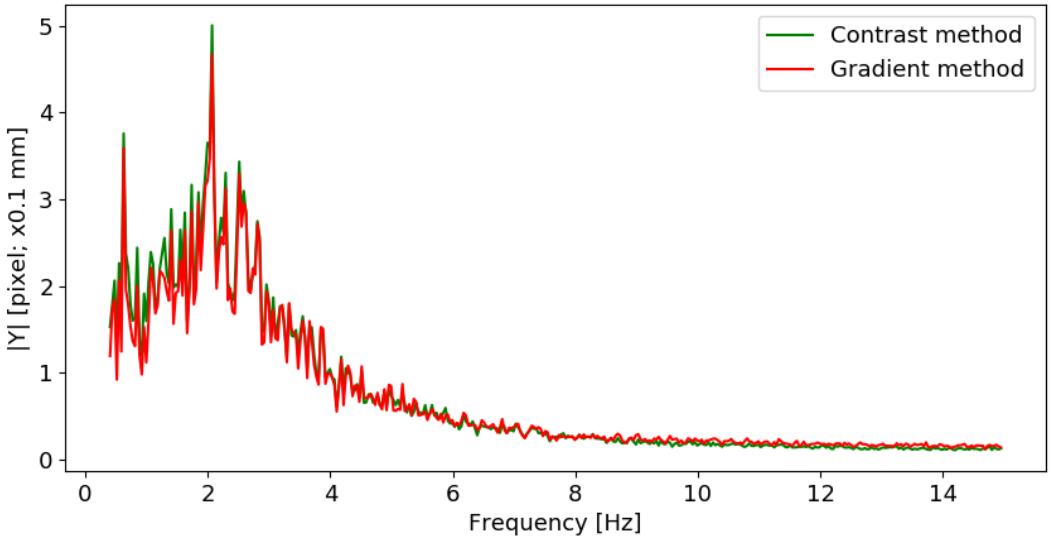

Figure 7. FFT spectrums for depths in the ROI for both methods in high surface aeration conditions.

For the contrast-based method, all statistical indicators demonstrate its failure to consistently capture the FSI in the low surface aeration conditions (Figure 9). On the other hand, gradient method had significant false detections in only 6 out of 1005 frames. These false positives resulted in somewhat underestimated minimal depths (Figure 9), but since the number of frames with such issues was below 0.6% of total, their effect on the average depth profile estimate is neglectable. Statistics for the gradient approach show that the time averaged depth increases approx. 2.6 times in the downstream direction. This ratio is somewhat larger when compared to the first experiment, due to a slight increase in the Froude number of the incoming flow (9.4 compared to the 8.3). Frequency spectrums are significantly different for the two methods (Figure 10). Spectrum of the contrast-based method shows an unusually high frequency content around 8 and 12 Hz, and higher amplitudes than gradient method across the entire spectrum. This can be attributed to the higher content of false positives which appear almost randomly in space and time along the jump. However, both methods still show the dominant oscillating frequency just above 2 Hz.

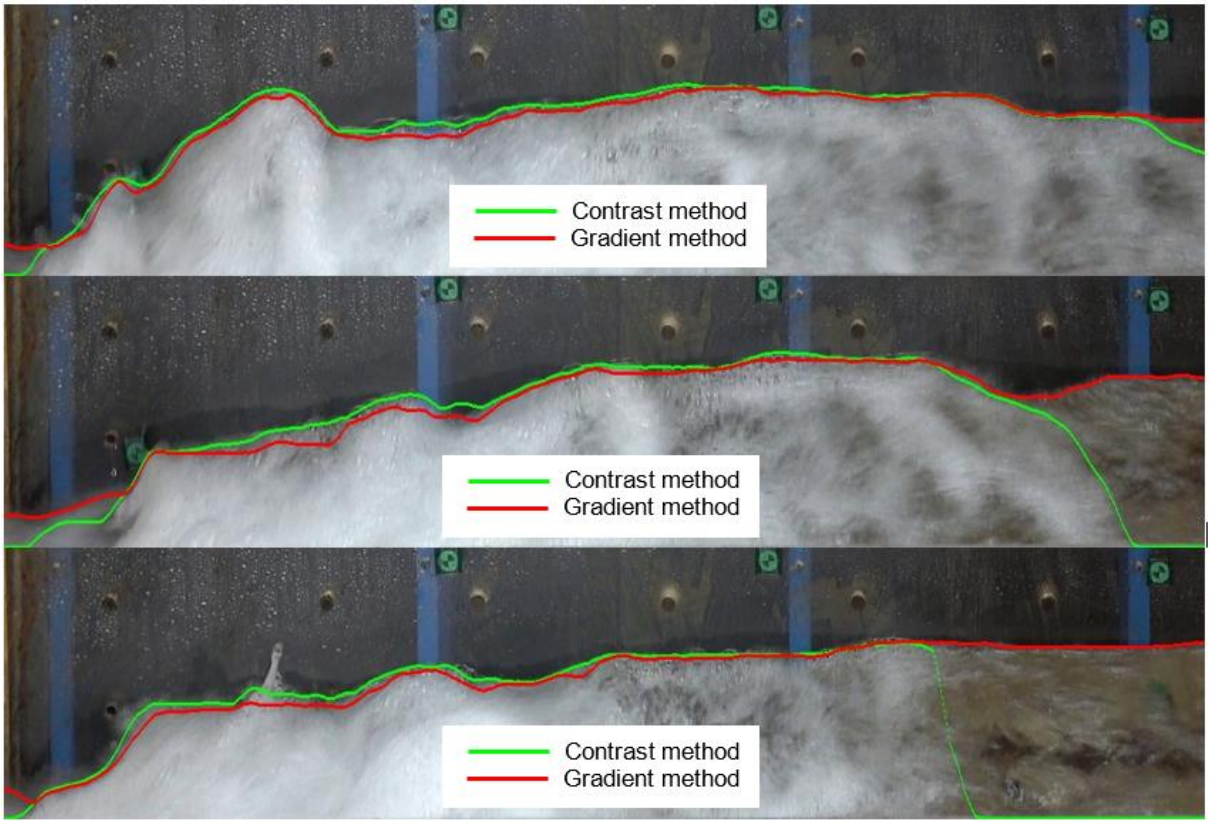

Figure 8. FSI detection for moderate to low surface aeration conditions at 20.7 L/s at different time instances.

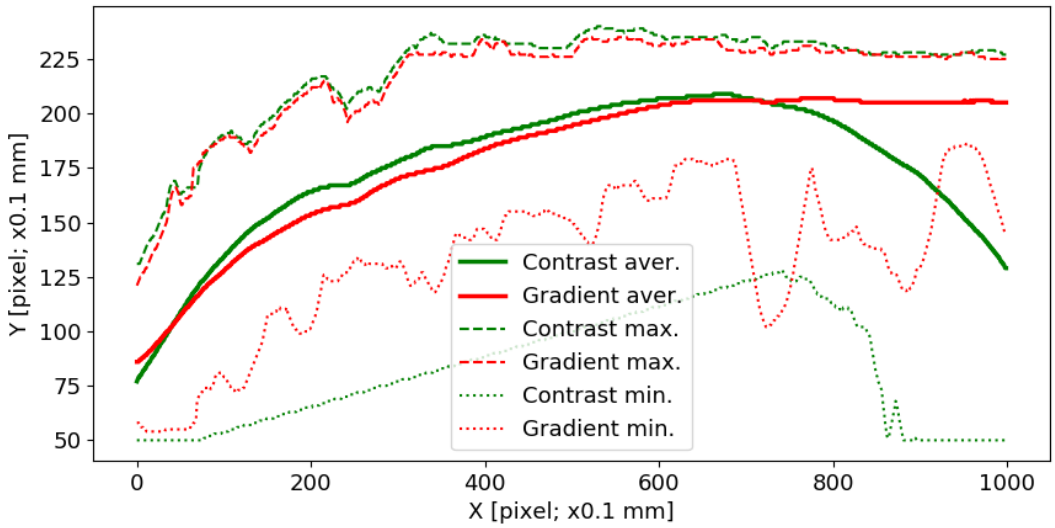

Figure 9. Statistics of the FSI profile along the hydraulic jump: averages, maximums, minimums along the hydraulic jump for both methods in moderate to low surface aeration conditions (1 pixel = 1 mm). Envelope of minimal depths for the contrast method is severely impacted by the gradient limiting filter.

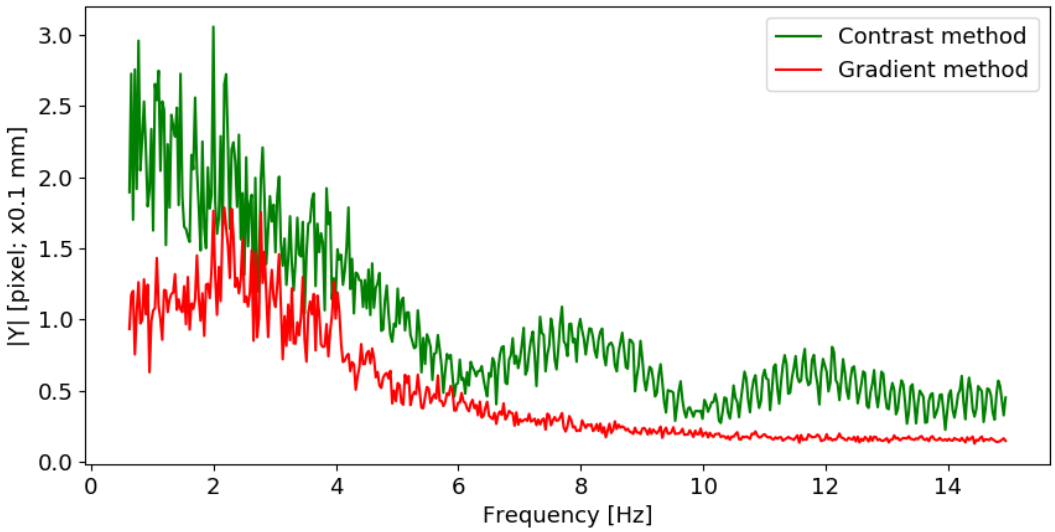

Figure 10. FFT spectrums for depths in the ROI for both methods in moderate to low surface aeration conditions.

Kernel size n in the Sobel-Feldman operator directly affects the accuracy of the FSI detection. Small kernel size (3x3, 5x5) will likely produce bias towards smaller image features including image noise, while if the kernel is too large it will potentially fail to notice the features of the FSI. Kernel should be of such size to detect only the main features in the image and should typically cover the real-world distance of a few centimeters. However, we have found that this parameter is far less case-specific than parameters of the contrast-based method and depends mostly on the pixel scale. A good estimate of the appropriate kernel size (for laboratory settings) should correspond to the real-world distance of 1 to 3 cm (e.g. if the pixel size corresponds to 1 mm in real-world setting, the first estimate of the kernel width can be between 11 and 31 pixels; kernel width/height must be an odd number).

However, it was found that both methods are sensitive to the flow transition at the toe of the hydraulic jump due to high degree of splashing and high flow velocity. Similarly, both algorithms tend to ignore sudden local depth increases due to splashing and droplets ejection, which can, at least partly, be attributed to the effects of used filters.

4 CONCLUSIONS

In this paper, an image processing method based on the gradient analysis using large kernel Sobel-Feldman operator, is presented for investigation of hydraulic jumps. This approach was compared to the contrast-based approach, used in majority of previous studies. Results show that the gradient method is more robust and accurate when compared to the contrast-based method. The proposed method was able to

reconstruct the free-surface interface without major artifacts, even in the presence of significant noise. The gradient detection method shows significantly better performance in the case of jumps with moderate and low surface aeration and/or if surface aeration changes drastically along the jump. However, the contrast-based approach has proven to be adequate for jumps with high surface aeration and when the surface aeration variability is low.

Future research should focus on the impact of different parameters on the quality of the FSI detection and subsequent depth estimation: camera framerate, camera recording angle, surface aeration intensity, flow velocity, etc. Additionally, different sizes and types of gradient detecting kernels, including non-square sized kernels, may improve the quality of detections. Further improvements to the proposed gradient method, based on deep-neural-networks, are being developed.

ACKNOWLEDGEMENTS

This work was supported by the Ministry of Education, Science and Technological Development of Serbia [grants TR37009 and TR37010].

REFERENCES

Bung, D. B. (2013). Non-intrusive detection of air–water surface roughness in self-aerated chute flows. *Journal of Hydraulic Research*, *51*(3), 322–329.

Hasan, I., Hies, T., Jose, E., Duester, R., Sattler, M., & Satzger, M. (2016). An Effective Camera Based Water level recording Technology for Flood Monitoring. *INTERPAEVENT*, 290–295. Lucerne, Switzerland.

IEC. (1999). *Amendment 1 Multimedia systems and equipment-Colour measurement and management-Part 2-1: Colour management-Default RGB colour space-sRGB*. Geneva, Switzerland.

Kucukali, S., & Chanson, H. (2008). Turbulence measurements in the bubbly flow region of hydraulic jumps. *Experimental Thermal and Fluid Science*, *33*(1), 41–53.

Leandro, J., Carvalho, R., Chachereau, Y., & Chanson, H. (2012). Estimating void fraction in a hydraulic jump by measurements of pixel intensity. *Experiments in Fluids*, *52*(5), 1307–1318.

Lennon, J. M., & Hill, D. F. (2006). Particle Image Velocity Measurements of Undular and Hydraulic Jumps. *Journal of Hydraulic Engineering*, *132*(12), 1283–1294.

Lin, Y., Lin, Y., & Han, J. (2018). Automatic water-level detection using single-camera images with varied poses. *Measurement*, *127*(May), 167–174.

Ljubičić, R., Zindović, B., Vojt, P., Pavlović, D., Kapor, R., Savić, L., … Savić, L. (2018). Hydraulic Jumps in Adverse-Slope Stilling Basins for Stepped Spillways. *Water*, *10*(4), 460.

MathWorks. (2019a). Camera Calibrator. Retrieved March 26, 2019, from https://www.mathworks.com/help/vision/ref/cameracalibrator-app.html

MathWorks. (2019b). What Is Camera Calibration? Retrieved March 26, 2019, from https://www.mathworks.com/help/vision/ug/camera-calibration.html

Misra, S. K., Thomas, M., Kambhamettu, C., Kirby, J. T., Veron, F., & Brocchini, M. (2006). Estimation of complex air-water interfaces from particle image velocimetry images. *Experiments in Fluids*, *40*(5), 764–775.

Montano, L., Li, R., & Felder, S. (2018). Continuous measurements of time-varying free-surface profiles in aerated hydraulic jumps with a LIDAR. *Experimental Thermal and Fluid Science*, *93*(January), 379–397.

Mossa, M., & Tolve, U. (1998). Flow Visualization in Bubbly Two-Phase Hydraulic Jump. *Journal of Fluids Engineering*, *120*(1), 160.

Murzyn, F., & Chanson, H. (2009). Free-surface fluctuations in hydraulic jumps: Experimental observations. *Experimental Thermal and Fluid Science*, *33*(7), 1055–1064.

Nóbrega, J. D., Schulz, H. E., & Zhu, D. Z. (2014). Free surface detection in hydraulic jumps through image analysis and ultrasonic sensor measurements. *Hydraulic Structures and Society - Engineering Challenges and Extremes*, (June), 1–8.

Parasuraman, S. B., Eikaas, H. S., Tan, K. M., Predictive, P. R., & Quality, W. (2012). *Enhanced water-level detection by image processing*. (October 2015).

Sobel, I. (2015). *An Isotropic 3x3 Image Gradient Operator*.

Tomasi, C., & Manduchi, R. (1998). Bilateral filtering for gray and color images. *Sixth International Conference on Computer Vision (IEEE Cat. No.98CH36271)*, 839–846. Narosa Publishing House.

Viriyakijja, K., & Chinnarasri, C. (2015). Wave Flume Measurement Using Image Analysis. *Aquatic Procedia*, *4*(Icwrcoe), 522–531.

Yu, J., & Hahn, H. (2010). Remote Detection and Monitoring of a Water Level Using Narrow Band Channel. *Journal of Information Science and Engineering*, *26*, 71–82.